Free-Drifting Icebergs: Hot Spots of Chemical and Biological Enrichment in the Weddell Sea

Kenneth L. Smith Jr.,[1]* Bruce H. Robison,[1] John J. Helly,[2] Ronald S. Kaufmann,[3] Henry A. Ruhl,[1] Timothy J. Shaw,[4] Benjamin S. Twining,[4] Maria Vernet[5]

The proliferation of icebergs from Antarctica over the past decade has raised questions about their potential impact on the surrounding pelagic ecosystem. Two free-drifting icebergs, 0.1 and 30.8 square kilometers in aerial surface area, and the surrounding waters were sampled in the northwest Weddell Sea during austral spring 2005. There was substantial enrichment of terrigenous material, and there were high concentrations of chlorophyll, krill, and seabirds surrounding each iceberg, extending out to a radial distance of ~3.7 kilometers. Extrapolating these results to all icebergs in the same size range, with the use of iceberg population estimates from satellite surveys, indicates that they similarly affect 39% of the surface ocean in this region. These results suggest that free-drifting icebergs can substantially affect the pelagic ecosystem of the Southern Ocean and can serve as areas of enhanced production and sequestration of organic carbon to the deep sea.

Atmospheric warming has been associated with retreating ice shelves and glaciers in the Antarctic over the past decade, particularly around the Antarctic Peninsula (*1*–*4*). The disintegration of ice shelves on both sides of the Antarctic Peninsula during the past 60 years has been attributed to atmospheric warming (*5*, *6*) and has contributed to the increased frequency of icebergs in the Weddell Sea (*7*).

Icebergs are very conspicuous features across the seascape of the Southern Ocean. They range in size from objects that are meters in diameter to large tabular structures that can exceed 300 km in length. In the Southern Ocean during the late 1980s, there were an estimated 200,000 icebergs with linear dimensions in the tens of meters to tens of kilometers (*8*, *9*). Iceberg shapes range from tabular to pinnacle forms, depending on their origin and state of decay by evaporation, melting, wave-induced erosion, and fracturing (*10*) during transit to their final ablation.

Little is known about the impact of free-drifting icebergs on the surrounding pelagic ecosystem. Anecdotal observations suggest that both depletion and enrichment of biological and chemical activity in the pelagic zone can be associated with icebergs. While stationary in a coastal region, a very large (~10,000 km^2) grounded iceberg with an associated faunal community (*11*) created shading and negatively influenced surface primary production (*12*). A smaller, free-drifting iceberg increased concentrations of iron and chlorophyll a in its wake (*13*). The density of acoustically reflective targets, believed to be zooplankton and micronekton, was twice as high under a free-drifting iceberg as compared with that of targets in surrounding open water in the Weddell Sea (*14*). Top predators, such as seabirds and seals, are also commonly associated with icebergs in the Southern Ocean (*15*–*17*).

Given the prevalence of icebergs in the Southern Ocean and the paucity of data concerning their impact on the surrounding ecosystem over their life span of months to years, we sought to address the following null hypothesis: As drifting islands, icebergs impart no significant ($P > 0.05$) chemical and biological characteristics to the surrounding ecosystem when compared with more peripheral waters some distance away.

Icebergs W-86 and A-52. We studied free-drifting icebergs during austral spring 2005 in the northwest (NW) Weddell Sea, an area of abundant icebergs that originate primarily from the ice shelves along the Antarctic Peninsula (Fig. 1A). Two drifting, tabular icebergs, located ~130 km apart and free of pack ice, were sampled along with the surrounding waters. One iceberg, W-86, was studied from 7 to 15 December 2005 as it traversed a total distance of 123 km (Fig. 1B). W-86 was <2 km long, with an aerial

[1]Monterey Bay Aquarium Research Institute (MBARI), 7700 Sandholdt Road, Moss Landing, CA 95039, USA. [2]San Diego Supercomputer Center, University of California, San Diego, La Jolla, CA 92093–0505, USA. [3]Marine Science and Environmental Studies Department, University of San Diego, 5998 Alcalá Park, San Diego, CA 92110, USA. [4]Department of Chemistry and Biochemistry, University of South Carolina, Columbia, SC 29208, USA. [5]Integrative Oceanography Division, Scripps Institution of Oceanography, University of California, San Diego, La Jolla, CA 92093–0218, USA.

*To whom correspondence should be addressed. E-mail: ksmith@mbari.org

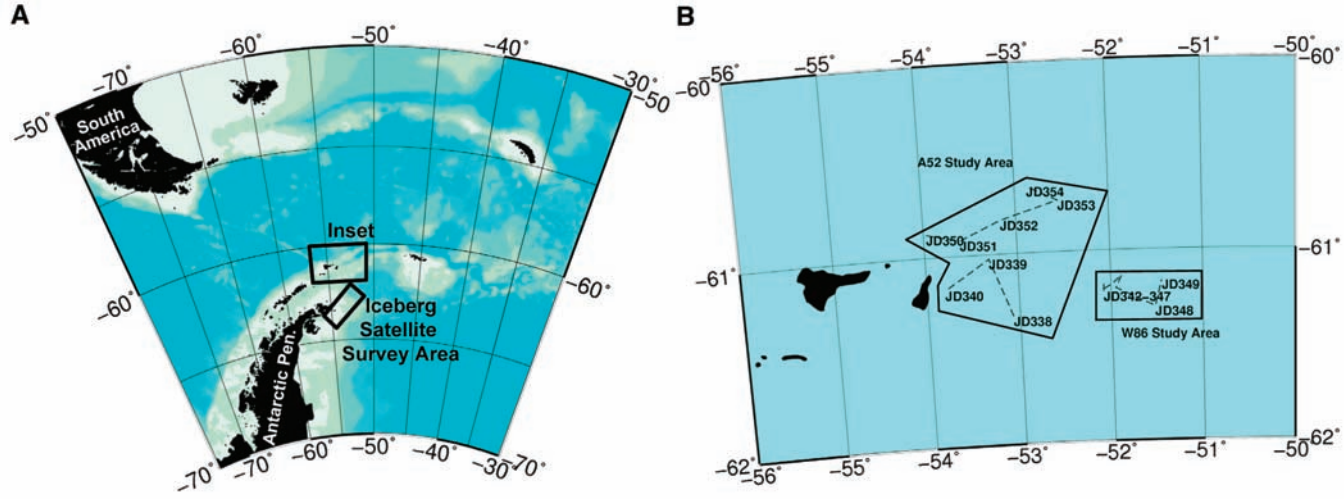

Fig. 1. Northeast extent of the Antarctic Peninsula and South Shetland Island chain, forming the western boundary of the NW Weddell Sea. (**A**) The study region including the shipboard study site [inset depicted in (B)] and the area of the processed SCANSAR-Wideband satellite image for analysis of iceberg number and size. (**B**) Enlarged inset from (A) outlining the study areas for iceberg A-52 to the east of Elephant and Clarence islands and for iceberg W-86 farther to the east. The trajectories of each iceberg, A-52 and W-86, are shown with Julian days (JD) indicated over the course of our study in austral spring 2005.

height of 41 m and a submerged depth of ≥300 m. This iceberg had an estimated aerial surface area of 0.12 km^2. A spiral sampling track was used to encircle the entire iceberg for ship-based surveys of iceberg structure, chlorophyll a, phytoplankton, zooplankton, and micronekton. We used a 10-m^2 opening-closing trawl [multiple opening-closing net and environmental sensing system (MOCNESS)]; a remotely operated vehicle (ROV) with a video camera; an underway flow-through conductivity-temperature-depth (CTD) instrument; a fluorometer; and a large volume pumping system (*18*). Spiral sampling began within 20 m of the iceberg and extended outward beyond 9 km, where the influence of the iceberg was not detectable. Superimposed on this sampling track was a series of CTD-rosette casts and stations where large volumes of water were pumped from depths ≤80 m.

For comparison, we studied a much larger iceberg that was clearly visible as a large feature in satellite images (RADARSAT and QuickSCAT). Iceberg A-52 was first sampled from 3 to 6 December 2005 before its temporary grounding off Clarence Island and was resampled from 16 to 21 December after again becoming free-drifting. The total distance traversed by A-52 over an 18-day period was 531 km (Fig. 1B). A-52 was oblong in shape, with a length of 21 km, an aerial height of 25 to 32 m, and a submerged depth of ≥230 m. The aerial surface area of A-52 was 300.8 km^2 during the first sampling period. However, during the second sampling period, the estimated surface area had decreased by an order of magnitude to 30.8 km^2, after obvious fracturing and ablation. Numerous large waterfalls cascaded from the crest of A-52, suggesting rapid melting across the extensive upper surface. A modified sampling program along the lengths of both sides of A-52, including CTD-rosette casts to 500 m depth, was initiated at parallel distances, extending out from 20 m to 9 km.

Meltwater contributions. Complex surface currents, with a strong diurnal tidal component modulated by inertial currents, imparted irregular spiraling rotations to both icebergs, while A-52 maintained an overall trajectory toward the northeast and W-86 moved primarily east (Fig. 1B) (*19*). Meltwater contributed to highly variable salinity in proximity to both icebergs (Fig. 2, A and B), with lowest salinities most prevalent in surface waters (Fig. 2, C and D). There was enrichment of short-lived ^{224}Ra (half-life = 3.7 days) in the surface waters adjacent to each iceberg. Excess ^{224}Ra (that fraction not supported by ambient parent isotopes) was chosen as an unambiguous terrigenous input. Because the only viable source of excess ^{224}Ra is the decay of ^{228}Th associated with terrigenous particles, the enrichment must indicate local input of ice-rafted detritus into the surrounding surface waters (typically <10 m depth) from meltwater. The sea-surface layer in areas proximal to both icebergs was enriched in excess ^{224}Ra when compared with deeper mixed-layer samples (30 to 80 m depth) that were at or below the detection limit (Fig. 2, E and F), precluding a deep upwelled source of enrichment. Surface enrichments decreased with increasing distance from the icebergs. The highest excess ^{224}Ra enrichment [5.0 disintegrations per minute (dpm) m^{-3}] was observed in water samples collected in brash ice broken off and immediately adjacent to iceberg W-86 (Fig. 2E). These samples also had the highest negative salinity anomaly as compared with samples from the surrounding surface waters, suggesting a meltwater source for the high ^{224}Ra. In contrast, lower excess ^{224}Ra activities were measured between 1 and 5 km from W-86 and from A-52 during the second sampling period (Fig. 2, E and F). We attribute the near "background" activities in some samples collected adjacent to A-52, during the first sampling period, to current-induced upwelling. The trend of decreasing excess ^{224}Ra activity with increasing distance from each iceberg suggests rapid melting and dispersion of the entrained terrigenous material, a potential source of iron to stimulate phytoplankton growth (*20*). Such inputs from free-drifting icebergs likely contribute to the elevated iron concentrations (~1 nM) measured in the Weddell Sea as compared with the extremely low-iron (≤0.1 nM), high-nutrient, low-chlorophyll waters of the Pacific and Indian sectors of the Southern Ocean (*21*).

Surface water concentrations of silicate, phosphate, ammonia, and nitrate revealed no significant pattern with distance from W-86 and A-52 due in part to limited sample sizes (fig. S1).

Phytoplankton community. Phytoplankton biomass, estimated as chlorophyll a integrated between the surface and 10-m depth samples from rosette bottle casts, was diluted in the immediate vicinity (<0.2 km) of iceberg W-86 and increased out to 1.0 km before declining again to significantly lower values ($P < 0.001$) beyond 3.7 km (Fig. 3, A and C, and table S1). A similar pattern, albeit at lower concentrations, was observed around A-52, with higher chlorophyll a concentrations in the immediate vicinity of the iceberg during the first sampling period (Fig. 3, B and D). Moderate concentrations of chlorophyll a occurred <0.25 km from iceberg A-52, with the highest concentrations around 0.5 km and background concentrations beyond 1.0 km. At locations adjacent to both icebergs, underway surface fluorometry measurements also exhibited the highest fluorescence values and variability, which generally decreased with in-

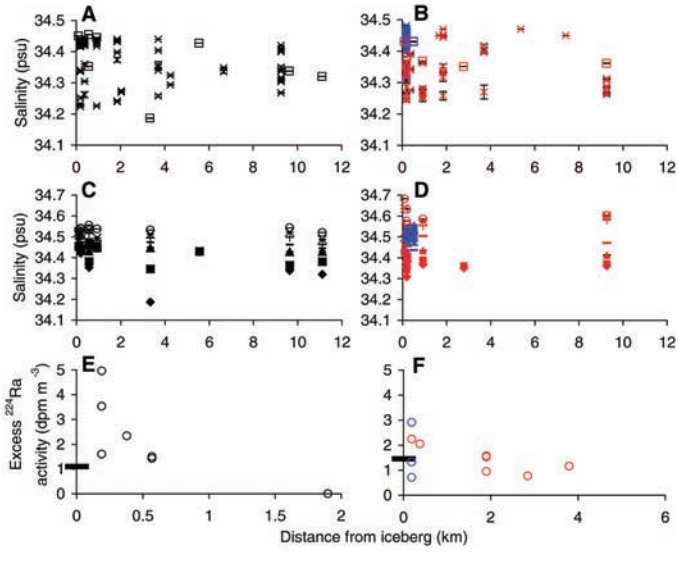

Fig. 2. Surface salinity and excess ^{224}Ra measured with increasing distance from icebergs W-86 and A-52. Black symbols represent measurements around W-86. The first and second sampling periods around A-52 are differentiated by blue and red symbols, respectively. (**A** and **B**) Mean surface salinity (± SE) at meter increments between 0 and 10 m depth determined from CTD casts [open squares; n = 10 measurements (W-86), n = 13 measurements (A-52)] and underway flow system salinity (intake at 5 m depth) determined at 1-min intervals for 5 min [crosses; n = 79 measurements (W-86), n = 100 measurements (A-52)]. The SE of each mean value is generally smaller than the representative symbol. psu, practical salinity units. (**C** and **D**) Mean salinity (± SE) determined from 10 CTD casts at W-86 and 13 casts at A-52 over the following depth intervals: 0 to 10 m (solid diamonds), 11 to 50 m (solid squares), 51 to 100 m (solid triangles), 101 to 200 m (dashes), 201 to 300 m (plus symbols), 301 to 400 m ("×" symbols), and 401 to 500 m (open circles). The SE for each mean value of each depth bin is generally smaller than the size of the representative symbol. (**E** and **F**) Excess ^{224}Ra in surface waters (0 to 10 m depth) with increasing distance from icebergs W-86 and A-52. The first sampling around A-52 (blue symbols) was more variable than the second sampling (red symbols), but the combined trends are similar. For comparison, nearshore sample activities (<10 km from the coastline of the Antarctic Peninsula; n = 7 measurements) are indicated by the black bar on the y axis. Average open ocean (≥100 km from any coastline in the Drake Passage; n = 6 measurements) and mixed-layer samples (30 to 80 m depth proximal to W-86 and A-52; n = 12 measurements) were at or below our detection limit of 0.6 dpm m^{-3}, as was the zero value for W-86 (*18*). [The detection limit was calculated as three (3σ) times our calculated counting error of 0.2 dpm m^{-3}. The error was determined with Poisson statistics on the total counts for each counting interval and propagated based on three counting intervals per sample.]

creasing radial distance (Fig. 3, A and B). The microphytoplankton (>20 μm) composed primarily of diatoms constituted the largest percentage of total chlorophyll a within 1.0 km of W-86 (53%) and A-52 (45%) (Fig. 3, C and D). Beyond a 3-km radius, the microphytoplankton fraction of total chlorophyll a was <24% around both icebergs. The high microphytoplankton biomass associated with W-86 and A-52 is similar to the enhanced biomass encountered in eutrophic areas near the edge of the seasonal pack ice (*22*) or during iron enrichment experiments (*23*, *24*).

Ice-associated community. The submerged sides of W-86 frequently had a reticulated surface, which consisted of indentations (ablation pockets) ~6 to 8 cm across and 1 to 2 cm deep. In the ridges between the indentations were small fragments of volcanic rock that served as attachment surfaces for tufted benthic diatoms, dominated by *Biddulphia aff. punctata*, with associated ciliates and foraminiferans. These diatom communities ranged from the surge-exposure depth of 8 m down to 60 m. Below this depth, there were no obvious signs of epibiota. Juvenile icefish (Channichthyidae) and polychaetes (Polynoidae), associated with pockets and folds in the ice surface, were observed by ROV video but were not collected.

The submerged structural characteristics of A-52 were more diverse than those of W-86, including caves, "subtidal" terraces, scoured areas, and apparent precursor or eroded stages of the reticulated indentations. In one area, a sharp edge led to the suspected underside of the iceberg at 230 m depth. Antarctic krill (*Euphausia superba*) occurred abundantly in association with many substrate forms, including the reticulated surface with attached diatom communities and caves that extended deep into the iceberg's interior. Ctenophores, siphonophores, and chaetognaths were also observed by ROV video in the water adjacent to the ice surface around both icebergs. Extensive expanses of attached diatoms, dominated by *Nitzschia aff. decipiens*, were also present on A-52, aligned as on W-86, between the reticulated indentations in the ice surface (fig. S2). The densest concentrations of these attached algal communities occurred on a flared terrace of the iceberg broadly exposed to downwelling light.

Macrozooplankton and micronekton community. Abundance of macrozooplankton and micronekton, dominated by *E. superba* and the chaetognath *Pseudosagitta gazellae*, was highest within a 3.7-km radius but diminished with increasing distance from both icebergs to much lower background values (Fig. 3, E and F). A Mann-Whitney *U* test revealed a significant decrease ($P < 0.009$) in macrozooplankton and micronekton abundance between the near-field (≤3.7-km radius) and far-field (>3.7-km radius) around A-52 (table S1). Although a similar trend in abundance was associated with W-86, there was no significant difference ($P > 0.05$) between the near- and far-field. The displacement volume of macrozooplankton and micronekton, an estimate of biomass, was highest within 3.7 km of each iceberg, as compared with samples collected >3.7 km away (Fig. 3, G and H). There was a significant decrease ($P < 0.005$) in displacement volume between the near- and far-field surrounding A-52, but no significant difference ($P > 0.05$) in volume was detected between the near- and far-field surrounding W-86 (table S1). Gelatinous zooplankton, especially medusae and siphonophores, were present in higher densities at A-52 than at W-86. In contrast, chaetognaths

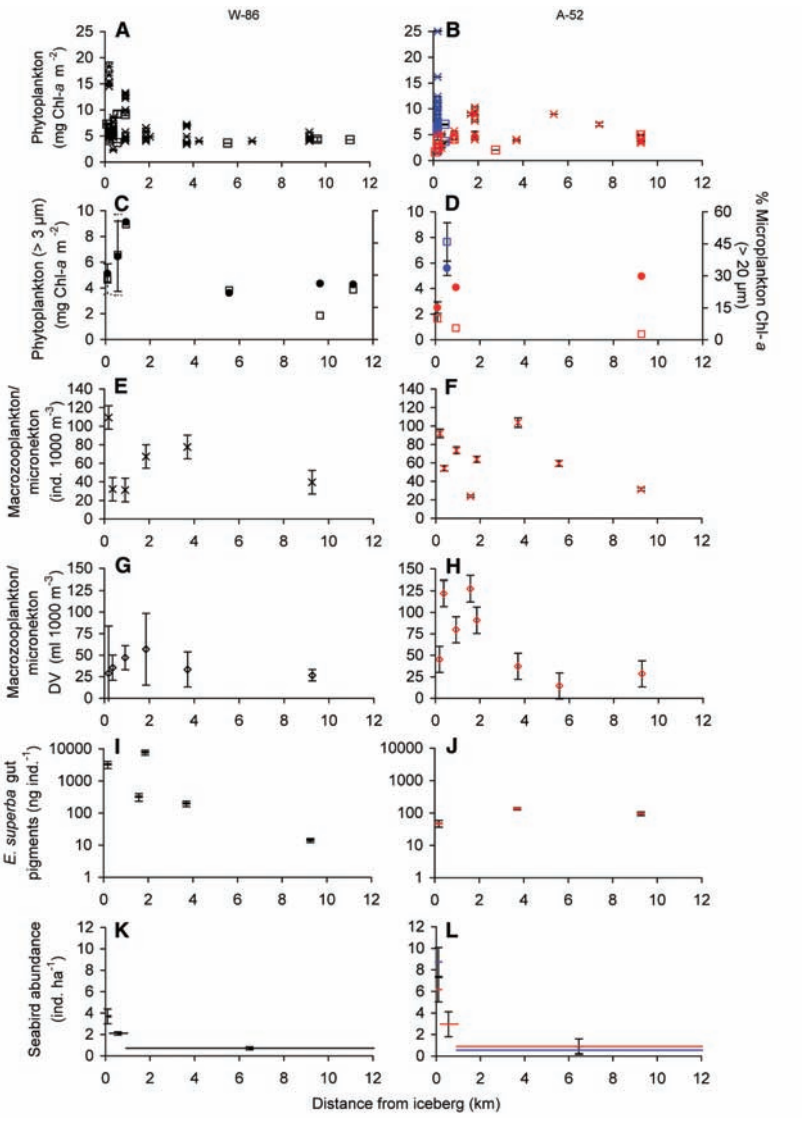

Fig. 3. Pelagic community characteristics as a function of distance from icebergs W-86 and A-52. Black symbols represent measurements around W-86. The first and second sampling periods around A-52 are differentiated by blue and red symbols, respectively. (**A** and **B**) Mean phytoplankton chlorophyll a concentrations (± SE) in filtered size fraction >3 μm integrated from 0 to 10 m depth [open squares; $n = 9$ measurements (W-86), $n = 13$ measurements (A-52)] and chlorophyll a determined from underway fluorometry [crosses; $n = 79$ measurements (W-86), $n = 100$ measurements (A-52)]. SE values of each mean are generally within the bounds of each symbol. (**C** and **D**) Mean chlorophyll a concentration for phytoplankton >3 μm for 0 to 10 m depth (solid circles ± SE) and the percent of that chlorophyll a associated with microphytoplankton >20 μm in size (open squares ± SE). (**E** and **F**) Macrozooplankton and micronekton abundance (mean ± SE) including all taxa. Fauna counted from collections made with a 10-m^2 opening-closing net system with six nets (MOCNESS) towed from ~1100 to 1400 hours (*18*). ind., individuals. (**G** and **H**) Macrozooplankton and micronekton displacement volume (DV) (mean ± SE) for all taxa combined. Fauna were collected as described above, and wet displacement volume was determined shipboard with fresh specimens. (**I** and **J**) Phytopigment analysis of guts from *E. superba*, the dominant macrozooplankton and micronekton species associated with W-86 ($n = 48$ specimens) and A-52 ($n = 39$ specimens). Chlorophyll a is represented by solid circles (mean ± SE) and phaeopigments are represented by "×" symbols (mean ± SE). (**K** and **L**) Pelagic seabird abundance for three aerial zones extending out from each iceberg (mean ± SE).

were more abundant in trawls around W-86 than in trawls near A-52.

In the guts of *E. superba* collected ≤3.7 km from W-86, significantly higher concentrations of phytopigments (chlorophyll a + phaeopigments) were measured, diminishing to lower levels at greater distance ($P < 0.001$; Fig. 3, I and J, and table S1). Consumption of phytoplankton by *E. superba* should contribute to localized export of particulate organic carbon in the form of fecal material (*25*) to greater depths surrounding icebergs. Gut phytopigment concentrations in *E. superba* surrounding W-86 were two orders of magnitude higher than concentrations measured in this species around iceberg A-52. No significant change in gut phytopigment concentration ($P > 0.05$) was detected in *E. superba* with distance from A-52.

Seabird community. Pelagic seabirds were significantly higher in number within 0.9 km of W-86 ($P < 0.001$) and A-52 ($P < 0.001$) in comparison with seabird numbers observed at distances >0.9 km away (Fig. 3, K and L, and table S1). The number of bird species was greater, and community evenness was significantly lower ($P < 0.001$), at locations near W-86 and A-52 as compared with those values measured at positions away from both icebergs. Decreased evenness has previously been associated with the increased dominance of a specific ecological factor, such as resource availability (*26*). Cape petrels (*Daption capense*) were the most numerous bird species, whereas Antarctic fulmars (*Fulmarus glacialoides*) were less abundant and covaried in density with cape petrels. Wilson's storm petrels (*Oceanites oceanicus*) were observed occasionally but were not common.

Bioavailability of terrigenous material. It is clear from our study that icebergs W-86 and A-52 influenced the surrounding pelagic ecosystem, as reflected in elevated concentrations of ^{224}Ra and increased densities of phytoplankton, zooplankton, and pelagic seabirds. As drifting islands, icebergs impart substantial chemical and biological characteristics to the surrounding ecosystem when compared with more peripheral waters some distance away, thus disproving our null hypothesis. We speculate that the release of trace elements, such as iron, stimulates primary production that trophically sustains enhanced populations of krill and predatory seabirds.

We conducted phytoplankton culturing experiments to evaluate the bioavailability of trace metals associated with the iceberg-borne terrigenous material. The growth of the centric diatom *Thalassiosira weissflogii* was compared in media amended with no trace metals, a full complement of trace metals buffered with EDTA, or 10 mg per liter of media of fine terrigenous particles (<63 μm) collected from iceberg fragments adjacent to W-86 (*18*). Diatoms grown in metal-free media amended with iceberg-borne terrigenous material grew at a moderate specific rate of 0.49 per day (a doubling time of 1.4 days), reaching a concentration of 28,000 cells per ml by the end of the 10-day incubation (Fig. 4). In contrast, cells grown in media prepared without metals achieved one cell division before becoming severely metal-limited and slowly senescing for the remainder of the 10-day incubation period. The initial cell division was likely enabled by Fe and other bioactive metals (e.g., Mn, Cu, Zn) stored in the cells before resuspension in the metal-free media. These cultures served as a negative control, demonstrating the limited growth of these cells in trace metal–free media. The highest growth rates for *T. weissflogii* occurred in metal-replete media (Fig. 4) and were similar to those measured by other researchers for this isolate under metal-replete conditions (*27*).

Although isolated from a coastal environment, *T. weissflogii* has been used in numerous studies of Fe availability and uptake, and it is representative of a class of phytoplankton that comprises a critical component of the export production in the Southern Ocean. Previous studies with *T. weissflogii* concluded that the diatom was unable to directly access colloidal or particulate Fe (*28*, *29*), indicating that Fe must dissolve before transport across the cell membrane. Possible mechanisms of dissolution include thermal dissolution (*28*), photoreduction (*30*, *31*), and complexation with siderophores or similar organic ligands (*32*). Each of these mechanisms could occur in the culture flasks of the experiment or naturally in the Southern Ocean.

Population of icebergs. To address how large an "area of influence" was exerted by the two icebergs on the surrounding pelagic zone, we estimated the biological enrichment associated with W-86 and A-52 to be the aerial surface area of each iceberg, depicted as a circle, the radius of which was increased by an additional 3.7 km [the distance beyond which macrozooplankton and micronekton abundance and displacement volume decreased to apparent background levels (Fig. 3, E to H)]. The estimated enrichment area was 47.7 km^2 for W-86 and 577.2 km^2 for A-52. Whether these icebergs have an entrained area of influence or a much larger impact, including a "wake" of enrichment, is yet to be resolved.

Our results show that the estimated area of influence of icebergs W-86 and A-52 was quite extensive. To obtain a broader spatial perspective, we processed the RADARSAT SCANSAR–Wideband satellite image closest in location and time to our study sites (Fig. 1A; image number R15378; 22 Feb 2006). The area processed, 11,265 km^2, contained 962 detectable icebergs free of pack ice, each ≥0.01 km^2 in area (*18*). More than 99% of these icebergs were <0.85 km^2 in area. With an area of 0.12 km^2, W-86 falls within this size range, but A-52 was much larger (fig. S3A). The total area covered by all the icebergs, 50.8 km^2, was only 0.45% of the total area surveyed in the satellite image.

However, our study has shown that there is a zone of biological influence that can extend ~3.7 km in radius from icebergs in the >0.1-km^2 size range. To estimate this expanded zone of biological influence, we assumed that each of the >0.1-km^2 icebergs in the satellite image was circular in area; the radius of each circle was thus calculated and expanded by 3.7 km and then the new area was recalculated (fig. S3B). A total of 89 icebergs fell within this larger size range, and their combined area of influence was 4387 km^2, equaling 39% of the area surveyed in the satellite image. Obviously, this area of influence would increase substantially if the remaining 873 icebergs <0.1 km^2 were included in this analysis. These calculations strongly support the contention that free-drifting icebergs can have a very pronounced impact on the pelagic ecosystem. Furthermore, the proliferation of icebergs associated with global warming should markedly increase their influence on the Southern Ocean ecosystem.

Conclusions. We envision free-drifting icebergs in the Weddell Sea as hot spots of continual micronutrient release that sustain the accompany-

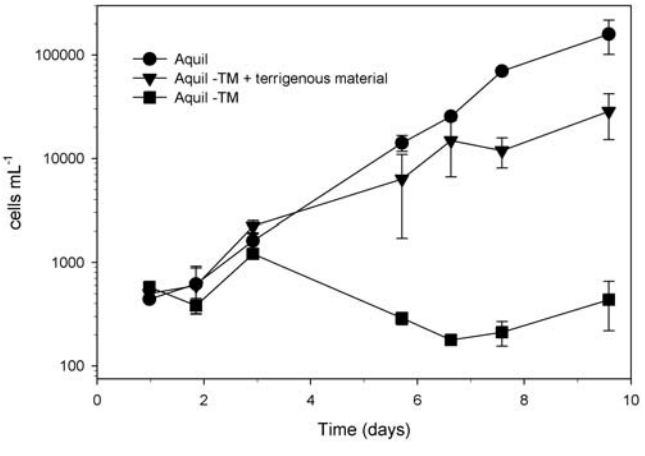

Fig. 4. Cell density of the diatom *T. weissflogii* grown in either metal-replete artificial seawater media (Aquil), media prepared without the addition of any trace metals (Aquil – TM), or media without added metals but amended with 10 mg of washed terrigenous material from iceberg W-86 per liter of media (Aquil – TM + terrigenous material). Cells were grown at 15°C under 300 μmol quanta m^{-2} s^{-1} on a 14:10 light: dark schedule. Cells were preacclimated to metal-deplete media for more than five generations before rinsing and resuspension into each treatment. Cell density was assayed with a Coulter Multisizer II electronic particle counter. Each data point is the mean (± SE) of triplicate cultures.

ing epibiotic and pelagic communities. These icebergs can be compared to estuaries that supply surrounding coastal regions with nutrients. In that respect, icebergs may be thought of as "Lagrangian estuaries," drifting through the Southern Ocean while enriching the surrounding pelagic zone. Our preliminary studies suggest that free-drifting icebergs and their associated communities could serve as areas of increased production and sequestration of organic carbon to the deep sea, a process unaccounted for in current global carbon budgets (*33*).

References and Notes

1. I. Velicogna, J. Wahr, *Science* **311**, 1754 (2006).
2. R. Thomas *et al.*, *Science* **306**, 255 (2004).
3. D. W. J. Thompson, S. Solomon, *Science* **296**, 895 (2002).
4. E. Rignot, S. S. Jacobs, *Science* **296**, 2020 (2002).
5. D. G. Vaughan, G. J. Marshall, W. M. Connolley, J. C. King, R. Mulvaney, *Science* **293**, 1777 (2001).
6. A. J. Cook, A. J. Fox, D. G. Vaughan, J. G. Ferrigno, *Science* **308**, 541 (2005).
7. T. A. Scambos, C. Hulbe, M. Fahnestock, J. Bohlander, *J. Glaciol.* **46**, 516 (2000).
8. R. N. Williams, W. G. Rees, N. W. Young, *Int. J. Remote Sens.* **20**, 3183 (1999).
9. O. Orheim, *Ann. Glaciol.* **11**, 205 (1988).
10. M. Kristensen, *Prog. Phys. Geogr.* **7**, 313 (1983).
11. G. Stone, *Nat. Geog. Mag.,* December 2001, pp. 36–52.
12. K. R. Arrigo, G. L. van Dijken, D. G. Ainley, M. A. Fahnestock, T. Markus, *Geophys. Res. Lett.* **29,** 10.1029/2001GL014160 (2002).
13. H. J. W. de Baar *et al.*, *Nature* **373**, 412 (1995).
14. R. S. Kaufmann *et al.*, *Mar. Biol.* **124**, 387 (1995).
15. D. G. Ainley, E. F. O'Connor, R. J. Boekelheide, *Ornithol. Monogr*. **32**, 1 (1984).
16. C. R. Joiris, *Polar Biol.* **11**, 415 (1991).
17. C. A. Ribic, D. G. Ainley, W. R. Fraser, *Antarct. Sci.* **3**, 181 (1991).
18. Materials and methods are available as supporting material on *Science* Online.
19. Shipboard acoustic doppler current profiler data taken during the cruise were analyzed by T. Chereskin (University of California, San Diego; Scripps Institution of Oceanography) to provide a description of surface currents surrounding icebergs A-52 and W-86.
20. B. M. Loscher, H. J. W. de Baar, J. T. M. de Jong, C. Veth, F. Dehairs, *Deep-Sea Res. II* **44**, 143 (1997).
21. H. J. W. de Baar, J. T. M. de Jong, in *The Biogeochemistry of Iron in Seawater*, D. R. Turner, K. A. Hunter, Eds. (Wiley, New York, 2001), pp. 123–253.
22. W. O. Smith, D. M. Nelson, *Science* **227**, 163 (1985).
23. K. H. Coale *et al.*, *Science* **304**, 408 (2004).
24. P. W. Boyd *et al.*, *Science* **315**, 612 (2007).
25. E. A. Pakhomov, P. W. Froneman, R. Perissinotto, *Deep-Sea Res. II* **49**, 1881 (2002).
26. G. Sugihara, L.-F. Bersier, T. R. Southwood, S. L. Pimm, R. M. May, *Proc. Natl. Acad. Sci. U.S.A.* **100**, 5246 (2003).
27. W. G. Sunda, S. A. Huntsman, *Mar. Chem.* **50**, 189 (1995).
28. M. L. Wells, N. G. Zorkin, A. G. Lewis, *J. Mar. Res.* **41**, 731 (1983).
29. H. W. Rich, F. M. M. Morel, *Limnol. Oceanogr.* **35**, 652 (1990).
30. T. D. Waite, F. M. M. Morel, *J. Colloid Interface Sci.* **102**, 121 (1984).
31. D. A. S. Finden, E. Tipping, G. H. M. Jaworski, C. S. Reynolds, *Nature* **309**, 783 (1984).
32. S. Kraemer, A. Butler, P. Borer, J. Cervini-Silva, *Rev. Mineral. Geochem.* **59**, 53 (2005).
33. I. Marinov, A. Gnanadesiker, J. R. Toggweiler, J. L. Sarmiento, *Nature* **441**, 964 (2006).

34. We thank all the shipboard scientific personnel on the research vessel *Laurence M. Gould* cruise LMG05-14A for excellent support, including R. Wilson, K. Reisenbichler, R. Sherlock, J. Ellena, M. Vardaro, K. Osborn, D. Chakos, J. Derry, L. Ekern, J. Kinsey, C. Koehler, and K. Noble. Captain R. Verret and his crew made sampling around icebergs a reality even under the most difficult conditions. The Raytheon Polar Services support group of S. Suhr-Sliester, J. Spillane, P. Fitzgibbons, K. Pedigo, J. Dolan, E. Roggenstein, and D. Elsberg provided excellent deck and laboratory support. D. Long (Brigham Young University) provided timely QuikSCAT images of the location of iceberg A-52 during our cruise. RADARSAT images of our study area were forwarded to the ship through Palmer Station. This research was supported by NSF grants ANT-0529815, ANT-0650034, and OCE-0327294, and by the David and Lucile Packard Foundation. We thank P. Penhale (NSF, Polar Programs) for having the foresight and courage to fund this speculative project. W. Moore and C. Hexel contributed to the ^{224}Ra analysis and data synthesis. C. Stoker of NASA/Ames Research Center loaned us the ROV, and H. Thomas at MBARI trained us in its operation.

Supporting Online Material

www.sciencemag.org/cgi/content/full/1142834/DC1
Materials and Methods
Figs. S1 to S3
Table S1
References

21 March 2007; accepted 4 June 2007
Published online 21 June 2007;
10.1126/science.1142834
Include this information when citing this paper.

The Product Space Conditions the Development of Nations

C. A. Hidalgo,[1]*† B. Klinger,[2]* A.-L. Barabási,[1] R. Hausmann[2]

Economies grow by upgrading the products they produce and export. The technology, capital, institutions, and skills needed to make newer products are more easily adapted from some products than from others. Here, we study this network of relatedness between products, or "product space," finding that more-sophisticated products are located in a densely connected core whereas less-sophisticated products occupy a less-connected periphery. Empirically, countries move through the product space by developing goods close to those they currently produce. Most countries can reach the core only by traversing empirically infrequent distances, which may help explain why poor countries have trouble developing more competitive exports and fail to converge to the income levels of rich countries.

Does the type of product that a country exports matter for subsequent economic performance? The fathers of development economics held that it does, suggesting that industrialization creates spillover benefits that fuel subsequent growth (*1*–*3*). Yet, lacking formal models, mainstream economic theory has been unable to incorporate these ideas. Instead, two approaches have been used to explain a country's pattern of specialization. The first focuses on the relative proportion between productive factors (i.e., physical capital, labor, land, skills or human capital, infrastructure, and institutions) (*4*). Hence, poor countries specialize in goods intensive in unskilled labor and land, whereas richer countries specialize in goods requiring infrastructure, institutions, and human and physical capital. The second approach emphasizes technological differences (*5*) and has to be complemented with a theory of what underlies them. The varieties and quality ladders models (*6*, *7*) assume that there is always a slightly more advanced product, or just a different one, that countries can move to, disregarding product similarities when thinking about structural transformation and growth.

Think of a product as a tree and the set of all products as a forest. A country is composed of a collection of firms, i.e., of monkeys that live on different trees and exploit those products. The process of growth implies moving from a poorer part of the forest, where trees have little fruit, to better parts of the forest. This implies that monkeys would have to jump distances, that is, redeploy (human, physical, and institutional) capital toward goods that are different from those currently under production. Traditional growth theory assumes there is always a tree within reach; hence, the structure of this forest is unimportant. However, if this forest is heterogeneous, with some dense areas and other more-deserted ones, and if monkeys can jump only limited distances, then monkeys may be unable to move through the forest. If this is the case, the structure of this space and a country's orientation within it become of great importance to the development of countries.

In theory, many possible factors may cause relatedness between products, that is, closeness between trees; such as the intensity of labor, land, and capital (*8*), the level of technological sophistication (*9*, *10*), the inputs or outputs involved in a product's value chain (e.g., cotton, yarn, cloth, and garments) (*11*), or requisite insti-

[1]Center for Complex Network Research and Department of Physics, University of Notre Dame, Notre Dame, IN 46556, USA. [2]Center for International Development, Kennedy School of Government, Harvard University, Cambridge, MA 02139, USA.

*These authors contributed equally to this work.
†To whom correspondence should be addressed. E-mail: chidalgo@nd.edu